JGR Oceans

RESEARCH ARTICLE
10.1029/2021JC017204

A Census of Eddies in the Tropical Eastern Boundary of the Indian Ocean

M. F. Azis Ismail[1], J. Ribbe[2], T. Arifin[3], A. Taofiqurohman[4], and D. Anggoro[5]

[1]Research Center for Oceanography, Indonesian Institute of Sciences, Jakarta, Indonesia, [2]School of Sciences, University of Southern Queensland, Toowoomba, QLD, Australia, [3]Marine Research Center, Ministry of Marine Affairs and Fisheries of Republic of Indonesia, Jakarta, Indonesia, [4]Department of Fisheries and Marine Science, Padjadjaran University, Bandung, Indonesia, [5]Department of Physics, Institut Teknologi Sepuluh Nopember, Surabaya, Indonesia

Abstract The Indo-Australian Basin (IAB) constitutes a crucial water route for the global ocean's circulation between the Pacific and Indian Oceans. Locally generated eddies contribute to the continued westward transport of water away from the IAB. In this paper, results from the first comprehensive regional ocean eddy census are discussed. A hybrid eddy census and tracking algorithm is used to analyze satellite altimetry data from 1993 to 2018. A total of 2,792 eddies were identified and tracked. Cyclonic eddies and anticyclonic eddies exhibit geographical segregation in terms of their dynamic characteristics. Larger amplitudes, radii, and absolute vorticities are associated with high eddy kinetic energy regions located in the vicinity of the South Java Current, South Equatorial Current, and Indonesian Throughflow. The eddies are grouped into three duration-based classifications providing the first systematic insight into understanding their physical characteristics, formation, and distribution in the IAB.

Plain Language Summary The Indo-Australian Basin (IAB) is one of the most important pathways for the exchange of water between the Pacific and Indian Oceans. In addition to ocean currents that move water westward, clockwise or anticlockwise rotating ocean eddies contribute to the transport from the IAB and toward the western Indian Ocean. The changing characteristics of these eddies are identified, quantified, and described in this paper. To do so, we use satellite data that reveal changes in sea surface height as an indicator for the presence of an eddy. The eddies are tracked from their genesis in the eastern IAB to their dissipation in the western Indian Ocean. In addition to the many small-scale features discovered for the first time, we found that one eddy existed for over a year and traveled a distance of more than 3,000 km during this time.

Key Points:

- Eddies identified and quantified in a new comprehensive census for the Indo-Australian Basin
- Newly identified hotspots for eddy activity identified in the eastern basin
- More than 41% of eddies detected than in previous surveys

Supporting Information:

Supporting Information may be found in the online version of this article.

Correspondence to:

M. F. Azis Ismail,
m.furqon.azis.ismail@lipi.go.id

Citation:

Azis Ismail, M. F., Ribbe, J., Arifin, T., Taofiqurohman, A., & Anggoro, D. (2021). A census of eddies in the tropical eastern boundary of the Indian Ocean. *Journal of Geophysical Research: Oceans*, *126*, e2021JC017204. https://doi.org/10.1029/2021JC017204

Received 21 JAN 2021
Accepted 28 MAY 2021

The copyright line for this article was changed on 16 JUN 2021 after original online publication.

1. Introduction

Eddies are omnipresent in the eastern boundary current regions of the world)s oceans (Bire & Wolfe, 2018; Chelton et al., 2011; Faghmous et al., 2015). They are the main source of kinetic energy in the oceans (Chelton et al., 2011), trap the eastern boundary currents near the coast (Bire & Wolfe, 2018), and contribute to mixing and transporting ocean properties over long distances (Azis Ismail & Ribbe, 2019; Faghmous et al., 2015; Henson & Thomas, 2008). The Indo-Australian Basin (IAB) located between 105°E–125°E and 6°S–20°S is the largest marginal sea along the southeastern tropical boundary of the Indian Ocean (Figure 1a). It encompasses a total area of about 2.5 million km^2, has an average depth of about 2,500 m, and is bounded in the north by the Java and Lesser Sunda Islands and in the south by the northwest Australian shelf. The IAB comprises the sole major route for the low-latitude interbasin transport from the Pacific into the Indian Ocean which is referred to as the Indonesian Throughflow (ITF). The warm and low-salinity water transferred by the ITF into the IAB plays a key role in the Indian and Pacific Oceans) heat budget (Sprintall et al., 2014).

The ITF enters the eastern edge of the IAB through an array of gaps within the Lesser Sunda Islands, namely the Lombok Strait, Ombai Strait, Sawu Sea, and Timor Passage. The outflow of the ITF along these straits induces large meanders (Feng & Wijffels, 2002) and high amplitude anticyclonic eddies (AEs) referred to as "teddies." These are eddies carrying ITF waters (Nof et al., 2002). The teddies can move westward and carry chlorophyll-rich water into the tuna-spawning zone of the IAB (Yu et al., 2015). Along the western boundary of the IAB, the mass and property exchange with the Indian Ocean takes place by means of several

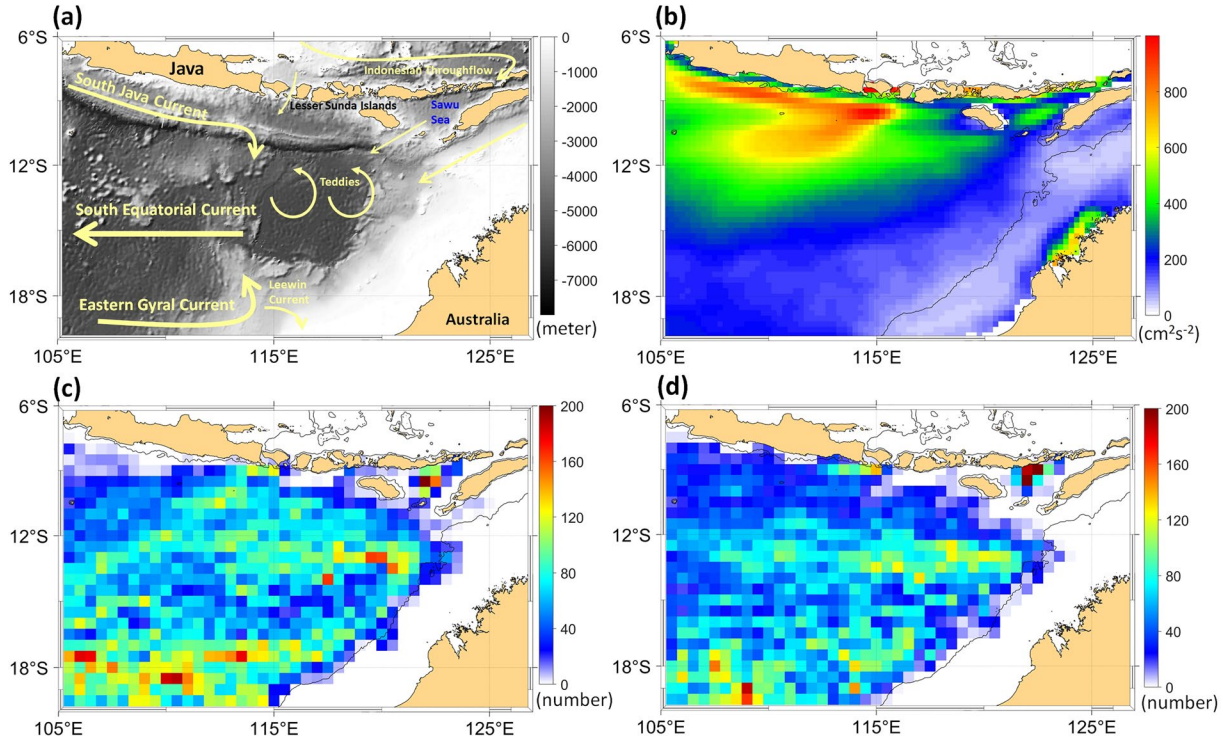

Figure 1. (a) Bathymetry of the Indo-Australian Basin (IAB) and schematic of surface currents. (b) Long term (January 1993 to December 2018) mean eddy kinetic energy ($cm^2\ s^{-2}$) in the IAB, and number of eddies detected in each 0.5° × 0.5° grid cell for (c) cyclonic eddies and (d) anticyclonic eddies. Black contour line represents the 500-m isobath.

large-scale currents: the South Java Current (SJC), the South Equatorial Current (SEC), and the Eastern Gyral Current (EGC). The SJC is the eastern boundary current off the south coast of Java that flows along the shelf-break toward the east before turning southward. To the south of the SJC resides the swift westward flow of the SEC. It forms the boundary between the large tropical and subtropical gyres of the Indian Ocean (Qu & Meyers, 2005). The EGC is a shallow eastward subtropical current which bifurcates partly into the SEC and partly feeds the southward flow of the Leeuwin Current (Feng & Wijffels, 2002).

The IAB is characterized by high mesoscale eddy activity. This appears to be the result of baroclinic instabilities that are associated with the SJC, SEC, and ITF (Feng & Wijffels, 2002; Jia et al., 2011; Z. Yu & Potemra, 2006). Eddies in the IAB play a key role in conveying the impact of the ITF on the region)s heat budget and are responsible for the termination of Indian Ocean Dipole events (Ogata & Masumoto, 2010, 2011). In addition, these eddies facilitate also the cross-shore transport of high chlorophyll water away from near coast to the open ocean waters (Yang et al., 2019). Yang et al. (2015, 2019) and Zhang et al. (2020) present eddy statistics for the western and southern section of the IAB, respectively, however no short-lived eddies (10–30 days) with radii <100 km were identified explicitly in those studies. As a result, a more comprehensive census of eddies across all temporal and spatial scales in the IAB is needed. Knowledge of eddies at different lifetimes (ranging from days to years) is essential in understanding the "genetic" history and "health" condition of eddies (Chen & Han, 2019). Thus, we expand in our study on Yang et al. (2015) and Zhang et al. (2020) by applying a hybrid eddy census and tracking algorithm to 26 years of merged sea level anomaly (SLA) data. This study results in the first systematic census of eddies in the IAB. Our objective is to conduct an eddy census, estimate surface characteristics of eddies as well as tracking their trajectories. Understanding the spatial and temporal evolution of eddies is essential in order to quantify their role in the mass and property exchanges across the IAB region and of similar processes operating in other eastern boundary regions.

2. Data and Methodology

Daily merged satellite altimetry multimission data including SLA and surface geostrophic currents from January 1993 to December 2018 are provided by the E.U. Copernicus Marine Environment Monitoring Service (CMEMS, https://marine.copernicus.eu/, last visited April 2021). The data are available at a spatial resolution of 0.25° (about 25 km) in latitude and longitude and were collated during the following satellite altimetry missions: Jason-1/2/3, Sentinel-3A, HY-2A, Saral/Altika, Cryosat-2, ERS1/2, TOPEX/Poseidon, ENVISAT, GFO, and ERS1/2.

In order to identify eddies, we utilized the hybrid eddy census algorithm of Halo et al. (2014). The hybrid algorithms is a robust eddy detection tool. It combines a geometric criterion with an Okubo-Weiss parameter resulting in a more reliable detection from SLA compared to only using an Okubo-Weiss parameter or a geometric criteria (Halo et al., 2014). In this hybrid method, the presence of a geostrophic eddy is defined as a coherent region detected within a closed SLA contour and an Okubo-Weiss parameter that is below a specified negative threshold value. The utilization of the Halo et al. (2014) method yields the location of an eddy)s core and its surface properties including amplitude, radius, and vorticity. In addition, this method is more reliable in detecting smaller eddies (mean diameter of 60–70 km) with lifetimes of <28 days (Lamont & van den Berg, 2020).

The Okubo-Weiss parameter is computed according to Okubo (1970) and Weiss (1991):

$$W = S_n^2 + S_s^2 - \xi^2 \tag{1}$$

$$S_n = \frac{\partial u}{\partial x} - \frac{\partial v}{\partial y},\ S_s = \frac{\partial v}{\partial x} + \frac{\partial u}{\partial y},\ \xi = \frac{\partial v}{\partial x} - \frac{\partial u}{\partial y} \tag{2}$$

where u (m s^{-1}) and v (m s^{-1}) are the horizontal velocity components in the x and y directions. The three parameters adopted are the following: the contour interval to identify closed loops of SLA is 0.02 m, the value of W is -2×10^{-12} s^{-2}, and a Hanning filter is applied twice on W as per Chelton et al. (2007, 2011) and Halo et al. (2014). An additional criterion is the maximum diameter of a closed SLA contour which is set to 300 km. This excludes the large ocean gyre-scale eddies from the census.

To track individual eddies during their lifetime, the eddy tracking algorithm adapted from Penven et al. (2005) is used. The method assumes that an eddy detected in one SLA map is the same eddy identified in the following SLA map if the distance in a nondimensional property space is at a minimum. This follows from the following equation (Penven et al., 2005):

$$X_{e1,e2} = \sqrt{\left(\left(\Delta X / X_0\right)^2 + \left(\Delta R / R_0\right)^2 + \left(\Delta \xi / \xi_0\right)^2\right)} \tag{3}$$

where ΔX (m) is the spatial range between the eddy cores X_{e1} and X_{e2}, ΔR (m) is the variation of diameter, $\Delta\xi$ (10^{-5} s^{-1}) is the variation of vorticity, X_0 is a characteristic length scale (25 km), R_0 is a typical eddy radius scale, and ξ_0 *is* a characteristic vorticity (10^{-5} s^{-1}). This tracking technique was successfully employed in other eddy studies including for the intensification zone of the East Australian Current (e.g., Azis Ismail & Ribbe, 2019), the Gulf of Guinea (e.g., Djakouré et al., 2014), the Mozambique Channel (e.g., Halo et al., 2014), and off Peru (e.g., Chaigneau et al., 2008).

Here, we identify and track persistent eddies with a lifetime of ≥10 days as this threshold would allow to quantify robust and "nonstationary" eddies (Faghmous et al., 2015). In addition, only eddies generated between 105°E–127°E and 6°S–20°S are tracked since this encompasses the IAB. Following Chen and Han (2019), we classified tracked eddies according to their lifetime into three categories: short lived (10 to 30 days), medium lived (from 31 to 365 days), and long lived (over 1 year).

3. Results and Discussion

3.1. Distribution of Mean Eddy Kinetic Energy and Eddy Characteristics

A band of maximum mean eddy kinetic energy (EKE) follows closely the northern IAB's shelf-break (Figure 1b, red shaded south of Java, >800 $cm^2\ s^{-2}$). It coincides with the flow of the SJC. Further in the east, the band arches toward the southwest at about 115°E approaching its minimum near 12°S and 108°E (Figure 1b). Also evident are bands of high mean EKE between 400 and 800 $cm^2\ s^{-2}$ that are located offshore in the vicinity of the SEC and the Lesser Sunda Islands (Figure 1b, shaded in green). The spatial pattern of two distinct regions of high mean EKE in bands south of Java to the Lesser Sunda Island indicates robust mesoscale variability in the vicinity of the SJC, SEC, and the ITF extension.

The separation into two regions of high EKE identified here is noted by Yang et al. (2015) as well, although their study area was located in the western region of the IAB. The extension of the high mean EKE belt throughout the outflow of the ITF explains the presence of teddies in which eddies transport ITF water westward (Nof et al., 2002) and advect chlorophyll-rich water further offshore (Yu et al., 2015). While a high EKE is supposed to be linked with a high total number of eddies (Pilo et al., 2015), the results from this eddy census do not overlap well with the spatial pattern of EKE (Figure 1b) for both cyclonic eddies (CEs) and AEs in Figures 1c and 1d, respectively. Areas of a higher total number of CEs and AEs are mainly observed in the vicinity of the SEC, across the eastern edge of the SJC near 115°E and 9°S, within the Sawu Sea, and the ITF region (Figures 1c and 1d). The elevated number of eddies in the IAB is maintained via the continuous formation of eddies by baroclinic instability of the surface current system or fronts in the IAB (Feng & Wijffels, 2002; Jia et al., 2011; Zhang et al., 2020).

In contrast to past research which indicates that the interaction of the SJC and the outflow of the ITF triggers only anticyclonic teddies (i.e., Nof et al., 2002), our results show that the ITF is also characterized by a high number of CEs. The pattern of high eddy density allows to identify the main hotspots (Figures 1c and 1d, >160 for CEs, >120 for AEs) of eddy activity in the IAB. These regions are newly identified hotspots which have been missed in previous surveys (Yang et al., 2015). However, the high total number of eddies does not mean that it is also a primary eddy formation region. In the case of the number of eddies in the IAB, our eddy identification method examines the number of eddies detected inside each spatial grid along the period January 1993 to December 2018. In addition, the eddy census method without eddy tracking (see below) does not take into consideration if a detected eddy is still the same eddy or not. Therefore, there is a possibility that an eddy can be counted more than once when propagating throughout the IAB.

An area of CEs and AEs with amplitudes >0.08 m, radii >80 km, and absolute vorticities $>8 \times 10^{-6}\ s^{-1}$ extends broadly along the confluence of the SJC, SEC, and outflow of the ITF (Figure 2). The region of large amplitudes, radii, and absolute vorticities aligns with that of the high mean EKE (Figure 1b). This indicates that large mean EKE relates better to amplitudes, radii, and absolute vorticities of both CEs and AEs near the vicinity of the SJC, SEC, and the ITF. The results from our census including eddies larger than 25 km in radius expand on Yang et al. (2015) where CEs and AEs radii of less than 100 km are not represented.

3.2. Eddy Origins and Trajectories

Most of the tracked eddies propagate westward toward the Indian Ocean and the resulting pattern of CEs and AEs trajectories is similar (Figure 3). The total number of tracked eddies is 2,793 (Table 1). On average, about 107 eddies are generated each year in the IAB. There are more tracked CEs than AEs. We identified that tracked eddies appeared to be ubiquitous throughout the IAB (Figure 3) in contrast to distinct regions of high and low EKE (Figure 1b). Our analysis is consistent with previous findings (Yang et al., 2015) in regards to eddy characteristics despite different eddy detection and tracking schemes applied. However, by including all of the IAB in our census, we find that about 41% of all eddies are detected initially east of 115°E (Table 1). This was the eastern limit of the study region investigated by Yang et al. (2015).

Short-lived eddies dominate the IAB with 1,751 eddies identified. This accounts for approximately 62.7% of all tracked eddies and includes 938 CEs and 813 AEs (Table 1). The eddies tend to dissipate not much further west than about 105°E (Figure 3a). Short-lived CEs (AEs) traveled a mean distance of 129.49 km (123.71 km), having a mean translation speed of 0.14 m s^{-1} (0.15 m s^{-1}), a mean amplitude of 0.04 m (0.05 m),

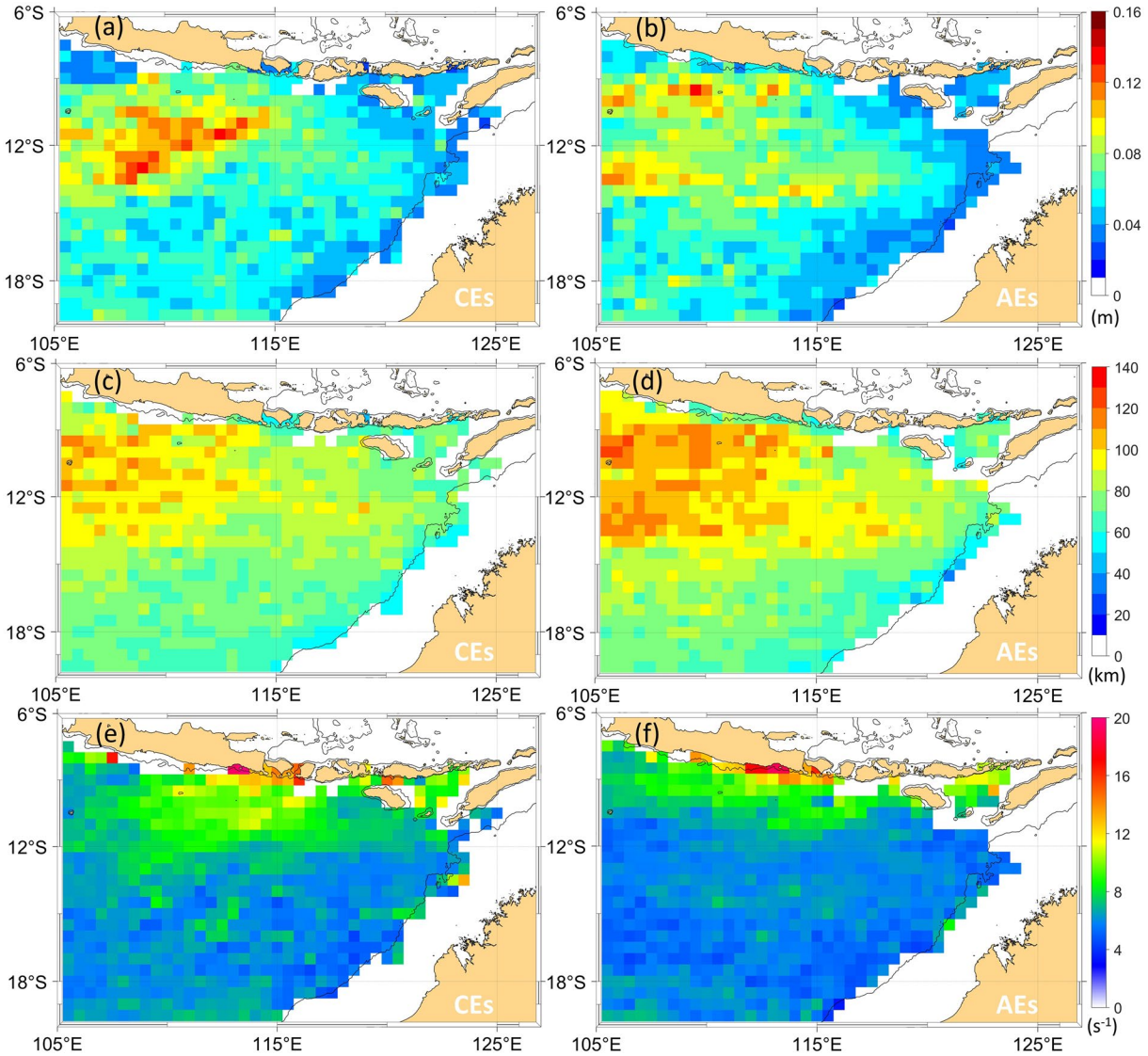

Figure 2. Distribution of eddy characteristics for cyclonic eddies (left) and anticyclonic eddies (right): (a and b) amplitudes (m), (c and d) radii (km), and (e and f) absolute vorticities (10^{-6} s^{-1}). Black contour line represents the 500-m isobath.

a mean radius of 72.41 km (74.85 km), and covered a mean surface area of 17.217 km^2 (18.516 km^2). Short-lived CEs and AEs have mean absolute vorticity of 6.51×10^6 and 6.45×10^6 s^{-1}, respectively (Table 1).

Medium-lived eddies propagate westward as well (Figure 3b) but are characterized by larger amplitudes, radii, and translation speeds than short-lived eddies. A total of 1,041 were tracked and contribute 37% of all tracked eddy. Of those, 557 and 484 were identified as CEs and AEs, respectively (Table 1). Before dissipating further in the western Indian Ocean, 136 CEs and 142 AEs crossed 105°E. Moreover, 5 CEs and 17 AEs traveled westward over a distance greater than 2,000 km and as far as 77°E. Mean translation speed, propagation distance, amplitude, radius, and size of AEs exceed that of CEs. An exception is the mean absolute vorticity. Translation speed and travel distance for medium-lived CEs is 0.15 m s^{-1} and 493.45 km while those for AEs are 0.17 m s^{-1} and 573.66 km. Mean amplitude of CEs (AEs) is 0.07 m (0.08 m) with a mean radius of 94.95 km (106.51 km). The mean surface area of CEs and AEs covered during their lifetime is 30,645 and 36,020 km^2, respectively. The medium-lived CEs have mean absolute vorticity of 6.51×10^6 s^{-1} while AEs have mean absolute vorticity of 6.45×10^6 s^{-1} (Table 1).

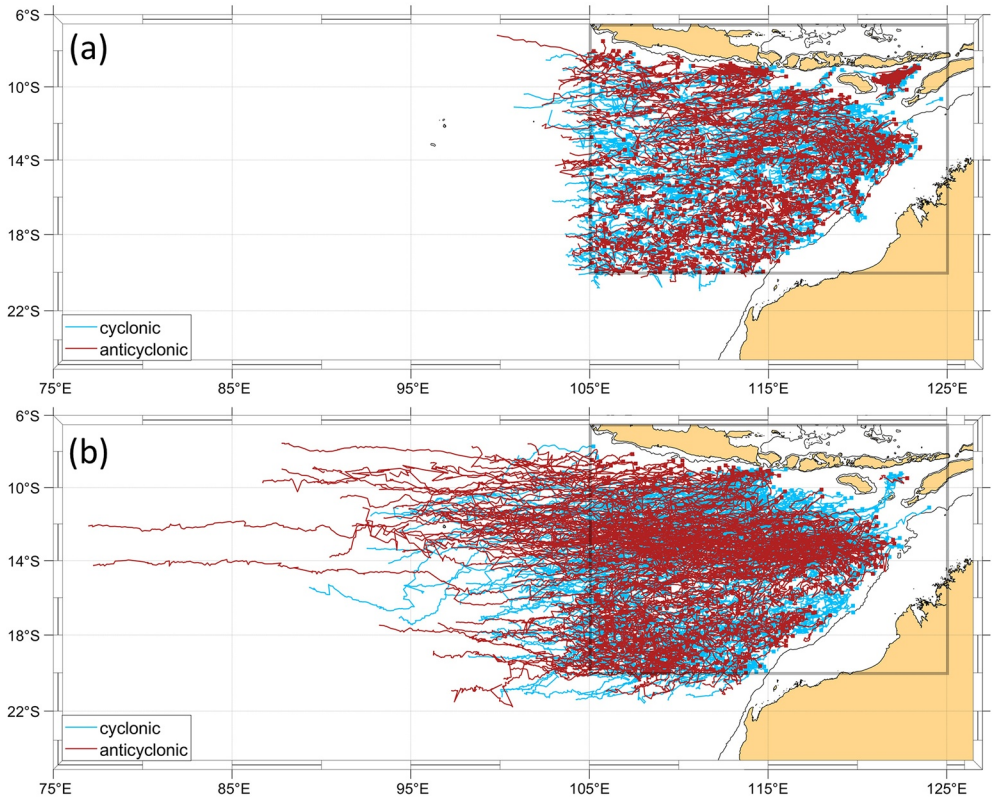

Figure 3. Trajectories of a cyclonic (blue) and anticyclonic (red) eddies from initial identification in the Indo-Australian Basin (IAB) to their termination sites west of the IAB: for (a) short-lived eddies and (b) medium-lived eddies. The eddy formation sites are marked by square. The 500-m isobath is indicated by thin black lines. The boxed area encompasses the IAB.

Only one long-lived (>365 days) eddy was identified and tracked. Its translation speed was about 30% slower than that of all other tracked eddies (Table 1). The eddy covered a distance of 3,047 km. Its mean amplitude and mean radius were 0.19 m and 106.51 km, and it occupied a mean surface area of 36.020 km^2. The spatial–temporal evolution of the long-lived CE and its main surface characteristics (i.e. amplitude, radius, and vorticity) is presented in Figure 4. A sequence of its location including SLA and associated surface geostrophic current allows to explore its evolution from genesis in the east to its dissipation west of 85°E.

Table 1
Cyclonic Eddies (CEs) and Anticyclonic Eddies (AEs) and Their Mean Characteristics

	Short-lived		Medium-lived		Long-lived	
Eddy lifetime	CEs	AEs	CEs	AEs	CEs	AEs
Number of tracked eddies[a]	938 (426)	813 (363)	557 (195)	484 (164)	1	–
Translation speed (m s^{-1})	0.14 ± 0.15	0.15 ± 0.17	0.15 ± 0.16	0.17 ± 0.18	0.11 ± 0.09	–
Propagation distance (km)	129.49 ± 87.36	123.71 ± 92.41	493.45 ± 389.37	574.66 ± 528.71	3,047.30	–
Amplitude (m)	0.04 ± 0.02	0.05 ± 0.02	0.07 ± 0.04	0.08 ± 0.04	0.19 ± 0.05	–
Core radius (km)	72.55 ± 15.38	74.71 ± 16.90	85.13 ± 21.87	94.95 ± 27.27	106.51 ± 11.13	–
Area (km^2)	17,278 ± 7,731	18,434 ± 9,114	24,273 + 13,327	30,654 ± 18,352	36,020 ± 7,475	–
Absolute vorticity (10^{-6} s^{-1})	6.51 ± 2.23	6.45 ± 2.49	6.93 ± 2.29	6.10 ± 1.77	12.36 ± 1.91	–

[a]Second number is eddies identified east of 115°E.

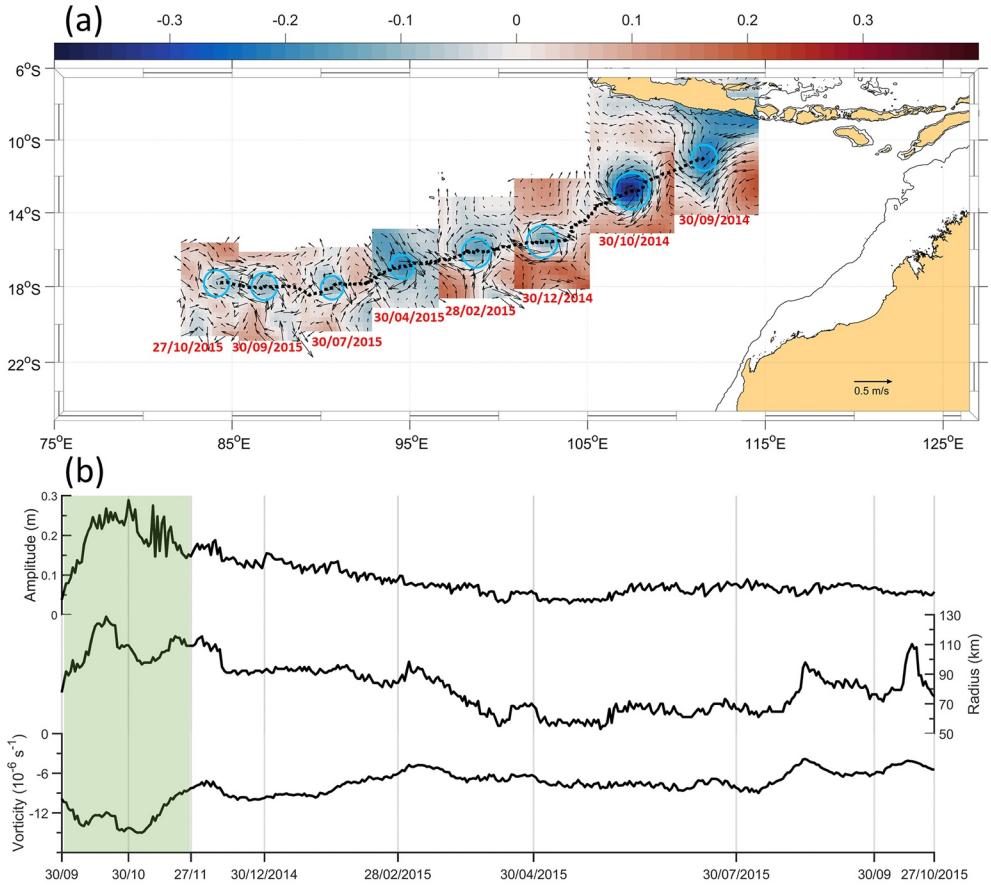

Figure 4. (a) Sequence of eddy evolution snapshot plotted against sea level anomaly (m) and geostrophic currents (m s^{-1}) maps for the long-lived cyclonic eddy (CE) generated in the Indo-Australian Basin (IAB) and (b) its time series of its amplitude, radius, and vorticity. The dates are presented at the bottom of each snapshot. Blue circles denote estimated radii of eddies. Black dotted lines represent propagation pathways. Green shading indicates the periods of the long-lived CE within the IAB. Thin black solid lines show the 500-m isobaths.

The eddy appeared to be spawned off a cyclonic circulation pattern close to the coast of Java with the eddy core situated near 111.56°E and 10.98°S on September 30, 2014 (Figure 4a). The formation of the long-lived CE is also confirmed by the presence of high chlorophyll-*a* than the surrounding offshore water (Figure S1). During the following 12 months, the eddy propagated westward in alignment with the mean pathway of the SEC. Amplitude, radius, and vorticity vary throughout its lifetime. Initially, a weak amplitude of 0.03 m, a radius of 77.65 km, and an absolute vorticity of 9.86×10^{-6} s^{-1} were detected. In the following month, the eddy grew into a much stronger eddy and reached 107.49°E and 12.82°S with a mean speed of about 0.14 m s^{-1} on October 30, 2014. Its amplitude, radius, and absolute vorticity increased during that period to 0.29 m, 109.44 km, and 1.09×10^{5} s^{-1}, respectively, and on November 27, 2014, the eddy exited the IAB near 105°E and 15°S. After crossing the border, it gradually weakened (Figure 4b). The eddy spent 70% of its lifetime outside the IAB. On December 30, 2014, it was located at 102.45°E and 15.58°S. Its amplitude, radius, and absolute vorticity had decreased to 0.13 m, 92.29 km, and 9.77×10^{-6} s^{-1}, respectively. The eddy was tracked until its dissipation after about 393 days. The tracked characteristics of the one long-lived CE suggest that the amplitude, radius, and vorticity in the IAB are larger than those for eddies that characterize the interior of the Indian Ocean (Figure 4).

4. Conclusion

This study provides the first systematic census of eddies, their surface characteristics as well as their propagation tracks in the IAB. Regions of high EKE link well with the regions of larger amplitudes, radii, and absolute vorticities for both CEs and AEs, particularly near the vicinity of the SJC, SEC, and the ITF outflows. A total of 2,793 individual tracked eddies were observed in the IAB, and over 40% of those are located in regions previously not investigated. Tracked CEs are more numerous than tracked AEs, and the former generally last longer. A total of 62.7% tracked eddies are short- and 37% are medium-lived eddies. Only one long-lived CE was identified and tracked. The duration-based classification of tracked eddies is a useful first step in gaining a comprehensive overview of eddy genesis in the IAB. In conclusion, this study finds that eddies are ubiquitous features of the IAB with highly variable characteristics and eddy activity hotspots are located in the very eastern regions of the basin. These have been identified for the first time for this so important region of the world ocean, connecting the Pacific and Indian Ocean via the ITF. CEs are important for the exchange and transport of heat and other ocean properties and future research needs to assess their contribution as previously done for AEs.

Conflict of Interest

The authors declare no conflicts of interest relevant to this study.

Data Availability Statement

Both altimeter and chlorophyll-*a* data are available via Copernicus Marine Environment Monitoring Service (CMEMS) information (https://marine.copernicus.eu).

Acknowledgments
This research was funded by the LIPI's COREMAP-CTI 2021–2022 no. 17/A/DK/2021. TA was supported by Marine Research Center, the Agency for Research & Human Resource Development, Ministry of Marine Affairs and Fisheries of Republic of Indonesia. We thank the two anonymous reviewers for their helpful comments on the manuscript.

References

Azis Ismail, M. F., & Ribbe, J. (2019). On the cross-shelf exchange driven by frontal eddies along a western boundary current during austral winter 2007. *Estuarine, Coastal and Shelf Science*, *227*, 106314. https://doi.org/10.1016/j.ecss.2019.106314

Bire, S., & Wolfe, C. L. P. (2018). The role of eddies in buoyancy-driven eastern boundary currents. *Journal of Physical Oceanography*, *48*(12), 2829–2850. https://doi.org/10.1175/JPO-D-18-0040.1

Chaigneau, A., Gizolme, A., & Grados, C. (2008). Mesoscale eddies off Peru in altimeter records: Identification algorithms and eddy spatio-temporal patterns. *Progress in Oceanography*, *79*(2–4), 106–119. https://doi.org/10.1016/j.pocean.2008.10.013

Chelton, D. B., Schlax, M. G., & Samelson, R. M. (2011). Global observations of nonlinear mesoscale eddies. *Progress in Oceanography*, *91*(2), 167–216. https://doi.org/10.1016/j.pocean.2011.01.002

Chelton, D. B., Schlax, M. G., Samelson, R. M., & de Szoeke, R. A. (2007). Global observations of large oceanic eddies. *Geophysical Research Letters*, *34*, L15606. https://doi.org/10.1029/2007GL030812

Chen, G., & Han, G. (2019). Contrasting short-lived with long-lived mesoscale eddies in the global ocean. *Journal of Geophysical Research: Oceans*, *124*, 3149–3167. https://doi.org/10.1029/2019JC014983

Djakouré, S., Penven, P., Bourlès, B., Veitch, J., & Koné, V. (2014). Coastally trapped eddies in the north of the Gulf of Guinea. *Journal of Geophysical Research: Oceans*, *119*, 6805–6819. https://doi.org/10.1002/2014JC010243

Faghmous, J. H., Frenger, I., Yao, Y., Warmka, R., Lindell, A., & Kumar, V. (2015). A daily global mesoscale ocean eddy dataset from satellite altimetry. *Scientific Data*, *2*, 1–16. https://doi.org/10.1038/sdata.2015.28

Feng, M., & Wijffels, S. (2002). Intraseasonal variability in the South Equatorial Current of the east Indian Ocean. *Journal of Physical Oceanography*, *32*(1), 265–277. https://doi.org/10.1175/1520-0485(2002)032<0265:IVITSE>2.0.CO;2

Halo, I., Backeberg, B., Penven, P., Ansorge, I., Reason, C., & Ullgren, J. E. (2014). Eddy properties in the Mozambique Channel: A comparison between observations and two numerical ocean circulation models. *Deep Sea Research Part II: Topical Studies in Oceanography*, *100*, 38–53. https://doi.org/10.1016/j.dsr2.2013.10.015

Henson, S. A., & Thomas, A. C. (2008). A census of oceanic anticyclonic eddies in the Gulf of Alaska. *Deep Sea Research Part I: Oceanographic Research Papers*, *55*(2), 163–176. https://doi.org/10.1016/j.dsr.2007.11.005

Jia, F., Wu, L., & Qiu, B. (2011). Seasonal modulation of eddy kinetic energy and its formation mechanism in the southeast Indian Ocean. *Journal of Physical Oceanography*, *41*(4), 657–665. https://doi.org/10.1175/2010JPO4436.1

Lamont, T., & van den Berg, M. A. (2020). Mesoscale eddies influencing the sub-Antarctic Prince Edward Islands Archipelago: Origin, pathways, and characteristics. *Continental Shelf Research*, *210*, 1–13. https://doi.org/10.1016/j.csr.2020.104257

Nof, D., Pichevin, T., & Sprintall, J. (2002). "Teddies" and the origin of the Leeuwin Current. *Journal of Physical Oceanography*, *32*(9), 2571–2588. https://doi.org/10.1175/1520-0485(2002)032<2571:TATOOT>2.0.CO;2

Ogata, T., & Masumoto, Y. (2010). Interactions between mesoscale eddy variability and Indian Ocean dipole events in the Southeastern tropical Indian Ocean—Case studies for 1994 and 1997/1998. *Ocean Dynamics*, *60*(3), 717–730. https://doi.org/10.1007/s10236-010-0304-4

Ogata, T., & Masumoto, Y. (2011). Interannual modulation and its dynamics of the mesoscale eddy variability in the southeastern tropical Indian Ocean. *Journal of Geophysical Research*, *116*, C05005. https://doi.org/10.1029/2010JC006490

Okubo, A. (1970). Horizontal dispersion of floatable particles in the vicinity of velocity singularities such as convergences. *Deep Sea Research and Oceanographic Abstracts*, *17*(3), 445–454. https://doi.org/10.1016/0011-7471(70)90059-8

Penven, P., Echevin, V., Pasapera, J., Colas, F., & Tam, J. (2005). Average circulation, seasonal cycle, and mesoscale dynamics of the Peru Current System: A modeling approach. *Journal of Geophysical Research*, *110*, C10021. https://doi.org/10.1029/2005JC002945

Pilo, G. S., Mata, M. M., & Azevedo, J. L. L. (2015). Eddy surface properties and propagation at Southern Hemisphere western boundary current systems. *Ocean Science*, *11*, 629–641. https://doi.org/10.5194/os-11-629-2015

Qu, T., & Meyers, G. (2005). Seasonal characteristics of circulation in the southeastern tropical Indian Ocean. *Journal of Physical Oceanography*, *35*(2), 255–267. https://doi.org/10.1175/JPO-2682.1

Sprintall, J., Gordon, A. L., Koch-Larrouy, A., Lee, T., Potemra, J. T., Pujiana, K., & Wijffels, S. E. (2014). The Indonesian seas and their role in the coupled ocean–climate system. *Nature Geoscience*, *7*(7), 487–492. https://doi.org/10.1038/ngeo2188

Weiss, J. (1991). The dynamics of enstrophy transfer in two-dimensional hydrodynamics. *Physica D: Nonlinear Phenomena*, *48*(2–3), 273–294. https://doi.org/10.1016/0167-2789(91)90088-Q

Yang, G., Yu, W., Yuan, Y., Zhao, X., Wang, F., Chen, G., et al. (2015). Characteristics, vertical structures, and heat/salt transports of mesoscale eddies in the southeastern tropical Indian Ocean. *Journal of Geophysical Research: Oceans*, *120*, 6733–6750. https://doi.org/10.1002/2015JC011130

Yang, G., Zhao, X., Li, Y., Liu, L., Wang, F., & Yu, W. (2019). Chlorophyll variability induced by mesoscale eddies in the southeastern tropical Indian Ocean. *Journal of Marine Systems*, *199*, 103209. https://doi.org/10.1016/j.jmarsys.2019.103209

Yu, W., Masumoto, Y., Hood, R. R., D)Adamo, N., McPhaden, M. J., Adi, R., et al. (2015). *The eastern Indian Ocean upwelling research initiative science plan and implementation strategy*. First Institution of Oceanography.

Yu, Z., & Potemra, J. (2006). Generation mechanism for the intraseasonal variability in the Indo-Australian basin. *Journal of Geophysical Research*, *111*, C01013. https://doi.org/10.1029/2005JC003023

Zhang, N., Liu, G., Liu, Q., Zheng, S., & Perrie, W. (2020). Spatiotemporal variations of mesoscale eddies in the southeast Indian Ocean. *Journal of Geophysical Research: Oceans*, *125*, e2019JC015712. https://doi.org/10.1029/2019JC015712